Advances in Applied Mathematics and Mechanics
Adv. Appl. Math. Mech., Vol. **9**, No. 6, pp. 1289-1311

DOI: 10.4208/aamm.2015.m1153
December 2017

Evaluating the Origin Intensity Factor in the Singular Boundary Method for Three-Dimensional Dirichlet Problems

Linlin Sun[1,2,3], Wen Chen[1,*] and Alexander H.-D. Cheng[3]

[1] *State Key Laboratory of Hydrology-Water Resources and Hydraulic Engineering, International Center for Simulation Software in Engineering and Sciences, College of Mechanics and Materials, Hohai University, Nanjing 210098, China*
[2] *Department of Computational Science and Statistics, School of Science, Nantong University, Nantong, Jiangsu 226019, China*
[3] *School of Engineering, University of Mississippi, University, MS 38677, USA*

Received 15 June 2015; Accepted (in revised version) 10 November 2016

Abstract. In this paper, a new formulation is proposed to evaluate the origin intensity factors (OIFs) in the singular boundary method (SBM) for solving 3D potential problems with Dirichlet boundary condition. The SBM is a strong-form boundary discretization collocation technique and is mathematically simple, easy-to-program, and free of mesh. The crucial step in the implementation of the SBM is to determine the OIFs which isolate the singularities of the fundamental solutions. Traditionally, the inverse interpolation technique (IIT) is adopted to calculate the OIFs on Dirichlet boundary, which is time consuming for large-scale simulation. In recent years, the new methodology has been developed to efficiently calculate the OIFs on Neumann boundary, but the Dirichlet problem remains an open issue. This study employs the subtracting and adding-back technique based on the integration of the fundamental solution over the whole boundary to develop a new formulation of the OIFs on 3D Dirichlet boundary. Several problems with varied domain shapes and boundary conditions are carried out to validate the effectiveness and feasibility of the proposed scheme in comparison with the SBM based on inverse interpolation technique, the method of fundamental solutions, and the boundary element method.

AMS subject classifications: 31C20, 34K28, 65N80, 65M70

Key words: Origin intensity factors, singular boundary method, boundary-type meshless method, potential problem, fundamental solution.

*Corresponding author.
Email: chenwen@hhu.edu.cn (W. Chen)

1 Introduction

The singular boundary method (SBM) is a recently developed strong-form meshless boundary collocation method [1, 2]. Like the boundary element method (BEM) [3–5] and method of fundamental solutions (MFS) [6–8], the SBM also employs the fundamental solutions of governing equation in the approximate representation and reduces the dimension of the problem by one. Unlike the BEM, the SBM, however, circumvents the meshing of the boundary. On the other hand, the SBM is different from the MFS, another strong-form meshless method, in that the SBM avoids the perplexing issue of auxiliary boundary outside the domain. To isolate the singularities of the fundamental solutions, the concept of origin intensity factors (OIFs) is introduced in the SBM which allows the source points to be placed on the boundary in coincidence with the collocation points. The calculation of the OIFs is essential in the implementation of the SBM.

The OIFs is first proposed in [1] and calculated by an inverse interpolation technique (IIT), in which a set of sample points should be placed inside the domain. The numerical experiments show that to some extent, the accuracy of the SBM with the IIT depends on the choice of sample nodes, so does the stability to the less extent. To remedy this problem, an improved scheme [9] is proposed in which the regularization technique of subtracting and adding-back [10, 11] used in the BEM is adopted to calculate the OIFs on Neumann boundary, while the inverse interpolation technique (IIT) is still used to calculate the OIFs on Dirichlet boundary. This improved method enhances the SBM solution accuracy while retaining all the merits of the SBM. The SBM has been successfully applied to solve many engineering problems such as heat conduction [12], potential [13], acoustic wave [14, 15], water wave [16], stokes flow [17], and biharmonic [18] problems. However, it is worth noting that the OIFs on Dirichlet boundary cannot be directly derived. When the IIT is adopted in the calculation of the OIFs on Dirichlet boundary, a system of linear equations is involved, which is time-consuming, especially for large-scale simulation.

Recently, a simple accurate formula [19, 20] to evaluate the OIFs on Dirichlet boundary is proposed for two-dimensional potential problems. In this new technique, the linear matrix system and the sample nodes inside domain for the OIFs in the IIT are both avoided. Consequently, the OIFs on Dirichlet boundary can be obtained directly and efficiently. The scheme can be extended to the problems governed by the Helmholtz and modified Helmholtz equations. However, such simple accurate formula for three dimensional Dirichlet problems is not reported in literature.

This paper proposes a new formulation to straightforwardly evaluate the OIFs on Dirichlet boundary in 3D problems and remedy the shortcomings in the IIT. This new strategy evaluates the OIFs by using the subtracting and adding-back technique based on the integration of the fundamental solution over the whole boundary. It is stressed that only the evaluation of the OIFs is involved with the numerical integration and the non-diagonal terms in the SBM interpolation matrix can simply be calculated via fundamental solution and the method is computationally far more efficient and mathematically simpler than the BEM.

The rest of this paper is organized as follows. In Section 2, we provide the formulation of the SBM for the 3D potential problems, introduce the new technique to obtain the OIFs on Dirichlet boundary, and discuss numerical integration of the fundamental solution over the whole boundary. In Section 3, several validation examples are presented to demonstrate the potential of the proposed method. The paper ends with a conclusion to summarize the presented work.

2 Formulation of singular boundary method

Let Ω be an open bounded domain for the problem of interest in $\mathbf{R}^3$ and $\Gamma=\partial\Omega$ denotes its boundary. Without loss of generality, we consider the 3D potential problem governed by

$$\nabla^2 u(\mathbf{x})=0, \quad \mathbf{x}\in\Omega, \tag{2.1}$$

subject to the following boundary conditions:

$$\begin{cases} u(\mathbf{x})=\hat{u}, & \mathbf{x}\in\Gamma_D, \\ q(\mathbf{x})=\nabla u(\mathbf{x})\cdot\mathbf{n}=\hat{q}, & \mathbf{x}\in\Gamma_N, \end{cases} \tag{2.2}$$

where

$$\nabla=\left(\frac{\partial}{\partial x_1},\frac{\partial}{\partial x_2},\frac{\partial}{\partial x_3}\right)$$

is the gradient operator, Γ_D and Γ_N denote the boundaries subject to the Dirichlet and Neumann boundary conditions, respectively, $\Gamma=\Gamma_N\cup\Gamma_D$, $\Gamma_N\cap\Gamma_D=\varnothing$, $\mathbf{n}$ represents the unit outward normal to the boundary, and $\hat{u}$ and $\hat{q}$ are the prescribed values.

In the SBM, the solutions for the problem are approximated by

$$u(\mathbf{x}_i)=\begin{cases} \displaystyle\sum_{j=1}^{N} a_j G(\mathbf{x}_i,\mathbf{s}_j)+c, & \mathbf{x}_i\in\Omega\backslash\Gamma, \\ \displaystyle\sum_{j\neq i}^{N} a_j G(\mathbf{x}_i,\mathbf{s}_j)+a_i\bar{u}_{ii}+c, & \mathbf{x}_i\in\Gamma_D, \end{cases} \tag{2.3}$$

and

$$q(\mathbf{x}_i)=\sum_{j\neq i}^{N} a_j\frac{\partial G(\mathbf{x}_i,\mathbf{s}_j)}{\partial\mathbf{n}_x}+a_i\bar{q}_{ii}, \quad \mathbf{x}_i\in\Gamma_N, \tag{2.4}$$

with the moment condition [21]

$$\sum_{j=1}^{N} a_j=0. \tag{2.5}$$

In the above equations, $\{a_j\}_{j=1}^N \cup \{c\}$ are unknown coefficients to be determined. $G(\mathbf{x}_i,\mathbf{s}_j)=\frac{1}{4\pi r(\mathbf{x}_i,\mathbf{s}_j)}$ denotes the fundamental solution, $r(\mathbf{x}_i,\mathbf{s}_j)$ is the Euclidean distance between collocation point $\mathbf{x}_i$ and source point $\mathbf{s}_j$ and N represents the number of the source points. It is noted that when the collocation point $\mathbf{x}_i$ coincides with the source point $\mathbf{s}_i$, the fundamental solution encounters so-called singularity at origin. And the OIFs $\bar{u}_{ii}$ and $\bar{q}_{ii}$ are introduced to isolate the singularities. In the following section, we focus on the derivation of OIFs.

2.1 The formulation of origin intensity factors on Neumann boundary

In most of previous works about the SBM, the OIFs on Neumann boundary are derived firstly by adopting a subtracting and adding-back technique [12,13] as follows:

$$\begin{aligned} q(\mathbf{x}_i) &= \sum_{j=1}^{N}\left(a_j-\frac{L_j}{L_i}a_i\right)\frac{\partial G(\mathbf{x}_i,\mathbf{s}_j)}{\partial \mathbf{n}_x}+a_i\sum_{j=1}^{N}\frac{L_j}{L_i}\cdot\frac{\partial G(\mathbf{x}_i,\mathbf{s}_j)}{\partial \mathbf{n}_x} \\ &= \sum_{j=1}^{N}\left(a_j-\frac{L_j}{L_i}a_i\right)\frac{\partial G(\mathbf{x}_i,\mathbf{s}_j)}{\partial \mathbf{n}_x}+\frac{a_i}{L_i}\sum_{j=1}^{N}\left(L_j\cdot\frac{\partial G(\mathbf{x}_i,\mathbf{s}_j)}{\partial \mathbf{n}_x}+L_j\cdot\frac{\partial G^{(e)}(\mathbf{x}_i,\mathbf{s}_j)}{\partial \mathbf{n}_s}\right), \end{aligned} \tag{2.6}$$

where

$$\sum_{j=1}^{N}\frac{L_j}{L_i}\cdot\frac{\partial G^{(e)}(\mathbf{x}_i,\mathbf{s}_j)}{\partial \mathbf{n}_s}=0, \tag{2.7}$$

with $\mathbf{x}_i=\mathbf{s}_i$ and L_j denotes area of the curved surface containing $\mathbf{s}_j$ as shown in Fig. 1. The detailed derivation of Eq. (2.7) is provided in Appendix A.

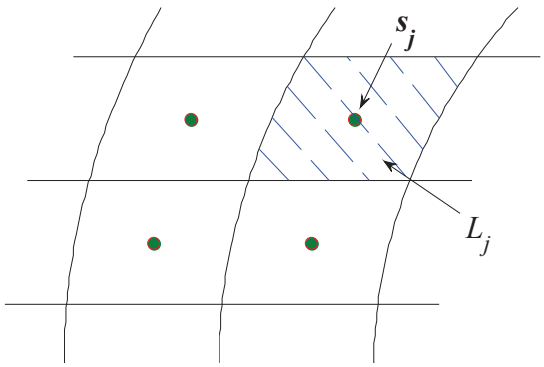

Figure 1: The source point and its corresponding discrete curved surface.

According to the dependency of the outward normal vectors on the double layer potentials of interior and exterior problems, one can obtain the following relationships [12, 22, 23]

$$\frac{\partial G(\mathbf{x}_i,\mathbf{s}_j)}{\partial \mathbf{n}_s}=-\frac{\partial G^{(e)}(\mathbf{x}_i,\mathbf{s}_j)}{\partial \mathbf{n}_s}. \tag{2.8}$$

Then, Eq. (2.6) can be recast as

$$q(\mathbf{x}_i)=\sum_{j\neq i}^{N}a_j\frac{\partial G(\mathbf{x}_i,\mathbf{s}_j)}{\partial \mathbf{n}_x}-a_i\left[\sum_{j\neq i}^{N}\frac{L_j}{L_i}\cdot\frac{\partial G(\mathbf{x}_i,\mathbf{s}_j)}{\partial \mathbf{n}_s}\right], \tag{2.9}$$

that is,

$$\bar{q}_{ii}=-\sum_{j\neq i}^{N}\frac{L_j}{L_i}\cdot\frac{\partial G(\mathbf{x}_i,\mathbf{s}_j)}{\partial \mathbf{n}_s}. \tag{2.10}$$

In this study, we also employ Eq. (2.10) to calculate the OIFs on the Neumann boundary.

2.2 New formulation of origin intensity factors on 3D Dirichlet boundary

Based on the computed OIFs on Neumann boundary, the OIFs for Dirichlet boundary conditions are calculated through the IIT in the SBM formulation [12]. One linear system need to be solved in the IIT which is time consuming for a large number of the boundary nodes. In addition, the sample solution used in the IIT may have certain influence on the numerical stability of the SBM in some cases. To alleviate these problems in the IIT, this paper proposes a new technique to evaluate the OIFs, which is based on the integration of the fundamental solution over the whole boundary. We have

$$\begin{aligned}u(\mathbf{x}_i)&=\sum_{j=1}^{N}a_jG(\mathbf{x}_i,\mathbf{s}_j)-a_i\left[\sum_{k=1}^{N}\frac{L_k}{L_i}\cdot G(\mathbf{x}_i,\mathbf{s}_k)-\frac{\Theta(\mathbf{x}_i)}{L_i}\right]\\&=\sum_{j\neq i}^{N}a_jG(\mathbf{x}_i,\mathbf{s}_j)+a_i[G(\mathbf{x}_i,\mathbf{s}_i)-G(\mathbf{x}_i,\mathbf{s}_i)]+a_i\left[\frac{\Theta(\mathbf{x}_i)}{L_i}-\sum_{k\neq i}^{N}\frac{L_k}{L_i}\cdot G(\mathbf{x}_i,\mathbf{s}_k)\right]\\&=\sum_{j\neq i}^{N}a_jG(\mathbf{x}_i,\mathbf{s}_j)+a_i\left[\frac{\Theta(\mathbf{x}_i)}{L_i}-\sum_{k\neq i}^{N}\frac{L_k}{L_i}\cdot G(\mathbf{x}_i,\mathbf{s}_k)\right],\end{aligned} \tag{2.11}$$

in which

$$\Theta(\mathbf{x}_i)=\int_{\Gamma}G(\mathbf{x}_i,\mathbf{s})d\Gamma(\mathbf{s}), \tag{2.12}$$

and

$$\sum_{k=1}^{N}\frac{L_k}{L_i}\cdot G(\mathbf{x}_i,\mathbf{s}_k)-\frac{\Theta(\mathbf{x}_i)}{L_i}=0, \tag{2.13}$$

where $\Theta(\mathbf{x}_i)$ denotes the accurate integration of the fundamental solution over the whole physical boundary and Eq. (2.13) is the discrete expression of Eq. (2.12) similar to Eq. (2.7). Thus

$$\bar{u}_{ii}=\frac{\Theta(\mathbf{x}_i)}{L_i}-\sum_{k\neq i}^{N}\frac{L_k}{L_i}\cdot G(\mathbf{x}_i,\mathbf{s}_k). \tag{2.14}$$

The above new formulation Eq. (2.14) avoids the calculation of the linear equations in the IIT. It is obvious that the key step in the implementation of the new method is to compute Eq. (2.12), which will be discussed in the next subsection.

2.3 Integration of the fundamental solution over the boundary

In this section, we consider the integration of the fundamental solution over several typical geometric boundaries.

Case 1: Spherical surface

Assume the boundary Γ is a spherical surface of radius R with the center at (x_1^0,x_2^0,x_3^0). Then an arbitrary point on the sphere surface can be expressed in spherical coordinates as

$$\mathbf{x}=(R\sin\theta\cos\phi+x_1^0,R\sin\theta\sin\phi+x_2^0,R\cos\theta+x_3^0),\quad 0\leq\theta<\pi,\quad 0\leq\phi<2\pi.$$

Because of the central symmetry of the sphere and the isotropy of the fundamental solution, the value of the integration $\Theta(\mathbf{x}_i)$ for all the collocation points on the boundary is the same. For the sake of simplicity, only the integration for the point $\mathbf{x}_0=(x_1^0,x_2^0,x_3^0+R)$ is calculated by

$$\Theta(\mathbf{x}_0)=\frac{1}{4\pi}\int_0^{2\pi}\int_0^{\pi}\frac{R^2\sin(\theta)}{\sqrt{2R^2(1-\cos\theta)}}d\theta d\phi=R. \tag{2.15}$$

Then, we have

$$\Theta(\mathbf{x})=R,\quad \mathbf{x}\in\Gamma. \tag{2.16}$$

Case 2: Cuboidal domain

Consider a cuboidal domain $[a_{\min},a_{\max}]\times[b_{\min},b_{\max}]\times[c_{\min},c_{\max}]$ with six piece wise smooth surfaces. For an arbitrary collocation point $\mathbf{x}_i=(x_1,x_2,x_3)$, the integration over

the surface $\{(x_1,x_2,x_3)|a_{\min}<x_1<a_{\max},\ b_{\min}<x_2<b_{\max},\ x_3=c_{\min}\}$ is given by

$$\begin{aligned} I(\alpha_0,\beta_0)&=\frac{1}{4\pi}\int_{\beta_{\min}}^{\beta_{\max}}\int_{\alpha_{\min}}^{\alpha_{\max}} 1\Big/\sqrt{(\alpha-\alpha_0)^2+(\beta-\beta_0)^2+\gamma^2}d\alpha d\beta \\ &=\frac{1}{4\pi}\left[F(\bar{\alpha}_{\max},\bar{\beta}_{\max})+F(\bar{\alpha}_{\min},\bar{\beta}_{\min})-F(\bar{\alpha}_{\max},\bar{\beta}_{\min})-F(\bar{\alpha}_{\min},\bar{\beta}_{\max})\right], \end{aligned} \tag{2.17}$$

where $\alpha_{\max}=a_{\max}$, $\alpha_{\min}=a_{\min}$, $\beta_{\max}=b_{\max}$, $\beta_{\min}=b_{\min}$, $\alpha_0=x_1$, $\beta_0=x_2$, $\gamma=c_{\min}-x_3$,

$$F(\alpha,\beta)=\alpha\ln(\beta+d)+\beta\ln(\alpha+d)-\gamma\operatorname{atan}\left(\frac{\alpha\beta}{\gamma d}\right),\quad d=\sqrt{\alpha^2+\beta^2+\gamma^2},$$

and

$$\bar{\alpha}_{\max}=\alpha_{\max}-\alpha_0,\quad \bar{\alpha}_{\min}=\alpha_{\min}-\alpha_0,\quad \bar{\beta}_{\max}=\beta_{\max}-\beta_0,\quad \bar{\beta}_{\min}=\beta_{\min}-\beta_0.$$

It is noted that the integrations over the other five surfaces can be analytically calculated through resetting the variables $\alpha_{\max}$, $\alpha_{\min}$, $\beta_{\max}$, $\beta_{\min}$, α_0, β_0, γ in Eq. (2.17). Then, $\Theta(\mathbf{x}_i)$ is the sum of the values of the integration over each surface.

Case 3: Cylindrical domain

For a hollow cylinder with x_3-axis as its central axis, the top and bottom surfaces are on $x_3=x_3^{\max}$ and $x_3=x_3^{\min}$, and the inner and outer radii are $\rho^{\min}$ and $\rho^{\max}$. Because the boundary is a rotate surface versus x_3-axis, the value of the integration Θ is the same for all the points on a circle in the plane perpendicular to x_3-axis and with the center point on x_3-axis. The point on boundary can be defined as

$$\mathbf{x}=(\rho\cos\theta,\rho\sin\theta,x_3),$$

with $x_{\min}\le x_3\le x_{\max}$, $0\le\theta<2\pi$ and $\rho=\rho_{\min}$ or $\rho_{\max}$ on inner and outer surfaces, and $\rho_{\min}\le\rho\le\rho_{\max}$, $0\le\theta<2\pi$ and $x_3=x_{\min}$ or $x_{\max}$ on bottom and top surfaces. Consider a collocation point $\mathbf{x}_0=(\rho_0,0,x_0)$ on the boundary. The integration $\Theta(\mathbf{x}_0)$ over the whole boundary can be divided into the integration over four piece wise surfaces, respectively.

For the inner and outer surfaces, we consider the following integral form

$$\begin{aligned} I_1(\mathbf{x}_i)&=\frac{1}{4\pi}\int_{-\pi}^{\pi}\int_{x_3^{\min}}^{x_3^{\max}}\bar{\rho}/\sqrt{(\bar{\rho}\cos\theta-\rho_0)^2+(\bar{\rho}\sin\theta-0)^2+(x_3-x_0)^2}dx_3d\theta \\ &=\frac{1}{4\pi}\int_{-\pi}^{\pi}f_1(\theta,x_3^{\max})-f_1(\theta,x_3^{\min})d\theta \\ &=I_1^{(1)}(\mathbf{x}_i)-I_1^{(2)}(\mathbf{x}_i), \end{aligned} \tag{2.18}$$

where

$$I_1^{(1)}(\mathbf{x}_i)=\frac{1}{2\pi}\int_0^{\pi}f_1(\theta,x_3^{\max})d\theta, \tag{2.19a}$$

$$I_1^{(2)}(\mathbf{x}_i)=\frac{1}{2\pi}\int_0^{\pi}f_1(\theta,x_3^{\min})d\theta, \tag{2.19b}$$

with $\bar{\rho}=\rho_{\min}$ on inner surface or $\bar{\rho}=\rho_{\max}$ on outer surface and

$$f_1(\theta,x_3)=\bar{\rho}\ln\left(x_3-x_0+\sqrt{\bar{\rho}^2+\rho_0^2-2\bar{\rho}\rho_0\cos\theta+(x_3-x_0)^2}\right).$$

Because it is difficult to obtain the analytical values of $I_1^{(1)}(\mathbf{x}_i)$ and $I_1^{(2)}(\mathbf{x}_i)$, the numerical integrations are employed to evaluate their values. Note that the function $f_1(\theta,x_3^{\max})$ in Eq. (2.19a) is singular when $\rho_0=\bar{\rho}$, $\theta=0$ and $x_0=x_{\max}$. To remove the singularity, we transform Eq. (2.19a) by

$$I_1^{(1)}(\mathbf{x}_i)=\frac{1}{2\pi}\int_0^{\pi}f_1(\theta,x_3^{\max})-f_2(\theta,x_3^{\max})d\theta+\frac{1}{2\pi}\int_0^{\pi}f_2(\theta,x_3^{\max})d\theta, \tag{2.20}$$

where

$$f_2(\theta,x_3)=\bar{\rho}\ln\left(x_3-x_0+\sqrt{(\bar{\rho}-\rho_0)^2+\bar{\rho}\rho_0\theta^2+(x_3-x_0)^2}\right),$$

and

$$\int_0^{\pi}f_2(\theta,x_3^{\max})d\theta=\theta f_2(\theta,x_3^{\max})|_0^{\pi}-\sqrt{\frac{\bar{\rho}}{\rho_0}}\left[F\left(\sqrt{b^2+\bar{\rho}\rho_0\pi^2},x_3^{\max}\right)-F(b,x_3^{\max})\right],$$

with

$$F(t,x_3)=\sqrt{t^2-b^2}-a\ln(t+\sqrt{t^2-b^2})-\sqrt{a^2-b^2}\ln\left(-2\frac{b^2+ta-\sqrt{(t^2-b^2)(a^2-b^2)}}{a+t}\right),$$

$$a=x_3-x_0,\quad b=\sqrt{(\bar{\rho}-\rho_0)^2+(x_3-x_0)^2}.$$

It can be found that when θ approaches 0,

$$\lim_{\theta\to0}\cos\theta=1-0.5\theta^2, \tag{2.21}$$

that is

$$\lim_{\theta\to0}\left[f_1(\theta,x_3^{\max})-f_2(\theta,x_3^{\max})\right]=0. \tag{2.22}$$

Thus there is no singularity for the integrand in the first term of the right side of the Eq. (2.20), which can be calculated through the Gauss quadrature

$$\int_0^{\pi}f_1(\theta,x_3^{\max})-f_2(\theta,x_3^{\max})d\theta=\frac{\pi}{2}\sum_{n=1}^{N_G}w_n\left[f_1(\hat{\theta}_n,x_3^{\max})-f_2(\hat{\theta}_n,x_3^{\max})\right], \tag{2.23}$$

where $\hat{\theta}_n=\frac{\pi}{2}(\kappa_n+1)$, κ_n and w_n are the nth Gauss point and the nth weighted function, respectively.

Similarly, $I_1^{(2)}(\mathbf{x}_i)$ in Eq. (2.19b) can be calculated by

$$\begin{aligned} I_1^{(2)}(\mathbf{x}_i) &= \frac{1}{2\pi}\int_0^{\pi} f_1(\theta, x_3^{\min}) - f_2(\theta, x_3^{\min})d\theta + \frac{1}{2\pi}\int_0^{\pi} f_2(\theta, x_3^{\min})d\theta \\ &= \frac{1}{2\pi}\left\{ \frac{\pi}{2}\sum_{n=1}^{N_G} w_n \left[f_1(\hat{\theta}_n, x_3^{\min}) - f_2(\hat{\theta}_n, x_3^{\min}) \right] \right. \\ &\quad \left. + \theta f_2(\theta, x_3^{\min})\big|_0^{\pi} - \sqrt{\frac{\bar{\rho}}{\rho_0}}\left[F\left(\sqrt{b^2 + \bar{\rho}\rho_0\pi^2}, x_3^{\min} \right) - F\left(b, x_3^{\min} \right) \right] \right\}. \end{aligned} \tag{2.24}$$

Then, we can obtain the integration over the inner or outer surface by substituting Eqs. (2.20) and (2.24) into Eq. (2.18).

Next, we consider the integration over the top and bottom surfaces as follows

$$\begin{aligned} I_2(\mathbf{x}_i) &= \frac{1}{4\pi}\left[\int_{-\rho_{\max}}^{\rho_{\max}} \int_{-\sqrt{\rho_{\max}^2 - x_1^2}}^{\sqrt{\rho_{\max}^2 - x_1^2}} g_1(x_1, x_2) dx_2 dx_1 - \int_{-\rho_{\min}}^{\rho_{\min}} \int_{-\sqrt{\rho_{\min}^2 - x_1^2}}^{\sqrt{\rho_{\min}^2 - x_1^2}} g_1(x_1, x_2) dx_2 dx_1 \right] \\ &= I_2^{(1)} - I_2^{(2)} - \frac{1}{4\pi}\left[g_3(x_1)\big|_{-\rho_{\max}}^{\rho_{\max}} - g_3(x_1)\big|_{-\rho_{\min}}^{\rho_{\min}} \right], \end{aligned} \tag{2.25}$$

where

$$I_2^{(1)} = \frac{1}{2\pi}\left[\int_{-\rho_{\max}}^{\rho_{\max}} g_2(x_1, \rho_{\max}) dx_1 \right], \tag{2.26a}$$

$$I_2^{(2)} = \frac{1}{2\pi}\left[\int_{-\rho_{\min}}^{\rho_{\min}} g_2(x_1, \rho_{\min}) dx_1 \right], \tag{2.26b}$$

$$g_1(x_1, x_2) = 1 \Big/ \sqrt{(x_1 - \rho_0)^2 + x_2^2 + (\bar{x}_3 - x_0)^2}, \tag{2.26c}$$

$$g_3(x_1) = 2(\bar{x}_3 - x_0)\arctan\left(\frac{x_1 - \rho_0}{\bar{x}_3 - x_0} \right) + (x_1 - \rho_0)\ln\left((x_1 - \rho_0)^2 + (\bar{x}_3 - x_0)^2 \right) - 2x_1, \tag{2.26d}$$

with $\bar{x}_3 = x_3^{\min}$ on the top surface or $\bar{x}_3 = x_3^{\max}$ on the bottom surface, and

$$g_2(x_1, \rho) = \ln\left(\sqrt{\rho^2 - x_1^2} + \sqrt{\rho^2 - x_1^2 + (x_1 - \rho_0)^2 + (\bar{x}_3 - x_0)^2} \right).$$

To avoid the singularity of $g_2(x_1, \rho)$, the transformation $x_1 = \rho\cos\theta$ is applied to Eqs. (2.26a) and (2.26b) leading to

$$I_2^{(1)} = \frac{1}{2\pi}\left[\int_0^{\pi} g_4(\theta, \rho_{\max}) d\theta \right], \tag{2.27a}$$

$$I_2^{(2)} = \frac{1}{2\pi}\left[\int_0^{\pi} g_4(\theta, \rho_{\min}) d\theta \right], \tag{2.27b}$$

where

$$g_4(\theta,\rho)=\rho\sin\theta\ln\left(\rho\sin\theta+\sqrt{\rho^2+\rho_0^2-2\rho\rho_0\cos\theta+(\bar{x}_3-x_0)^2}\right).$$

It is obvious that there is no singularity in $g_4(\theta,\rho)$ for $0\leq\theta\leq\pi$. The numerical integration $I_2^{(1)}-I_2^{(2)}$ can be calculated by the Gauss quadrature as:

$$I_2^{(1)}-I_2^{(2)}=\frac{1}{2\pi}\left[\frac{\pi}{2}\sum_{n=1}^{N_G}w_n\left[g_4(\hat{\theta}_n,\rho_{\max})-g_4(\hat{\theta}_n,\rho_{\min})\right]\right]. \tag{2.28}$$

Then, the integration $\Theta(\mathbf{x}_0)$ can be determined by using Eqs. (2.18) and (2.25). Also, the values of the integration for the points $\mathbf{x}=(\rho_0\cos\theta,\rho_0\sin\theta,x_0)$, $-\pi\leq\theta\leq\pi$ can be determined which are the same as $\Theta(\mathbf{x}_0)$.

Case 4: Smooth surface of arbitrary shape

Consider the problem domain surrounded by a second-order smooth surface which is represented by

$$\mathbf{x}=(X(\alpha,\beta),Y(\alpha,\beta),Z(\alpha,\beta)),\quad \alpha_{\min}\leq\alpha\leq\alpha_{\max},\quad \beta_{\min}\leq\beta\leq\beta_{\max}.$$

For a collocation point $\mathbf{x}_i=(X(\alpha_i,\beta_i),Y(\alpha_i,\beta_i),Z(\alpha_i,\beta_i))$, we have

$$\Theta(\mathbf{x}_i)=\frac{1}{4\pi}\int_{\beta_{\min}}^{\beta_{\max}}\int_{\alpha_{\min}}^{\alpha_{\max}}f(\alpha,\beta)d\alpha d\beta, \tag{2.29}$$

where

$$f(\alpha,\beta)=\frac{h(\alpha,\beta)}{\sqrt{[X(\alpha,\beta)-X(\alpha_i,\beta_i)]^2+[Y(\alpha,\beta)-Y(\alpha_i,\beta_i)]^2+[Z(\alpha,\beta)-Z(\alpha_i,\beta_i)]^2}},$$

with $h(\alpha,\beta)=\left|(X_{,\alpha},Y_{,\alpha},Z_{,\alpha})\times(X_{,\beta},Y_{,\beta},Z_{,\beta})\right|$, the Jacobian, $(\,)_{,\alpha}$ is the derivative with respect to α, and $\times$ denotes the symbol for cross product.

Because it is difficult to obtain the analytic integral value of Eq. (2.29), we focus on the numerical integration. Note that the function $f(\alpha,\beta)$ will become singular when (α,β) approaches (α_i,β_i). In order to facilitate the calculation, we need to transform Eq. (2.29) into the integration in term of a non-singular function. Firstly, we divided the integration into four parts as follows

$$\begin{aligned}\Theta(\mathbf{x}_i)=&1/4\pi\left[I_1+I_2+I_3+I_4\right]\\=&\frac{1}{4\pi}\left[\int_{\beta_i}^{\beta_{\max}}\int_{\alpha_i}^{\alpha_{\max}}f(\alpha,\beta)d\alpha d\beta+\int_{\beta_i}^{\beta_{\max}}\int_{\alpha_{\min}}^{\alpha_i}f(\alpha,\beta)d\alpha d\beta\right.\\&\left.+\int_{\beta_{\min}}^{\beta_i}\int_{\alpha_{\min}}^{\alpha_i}f(\alpha,\beta)d\alpha d\beta+\int_{\beta_{\min}}^{\beta_i}\int_{\alpha_i}^{\alpha_{\max}}f(\alpha,\beta)d\alpha d\beta\right].\end{aligned} \tag{2.30}$$

Then, with the transform $\alpha=\bar{\alpha}(\alpha_{\max}-\alpha_i)+\alpha_i$ and $\beta=\bar{\beta}(\beta_{\max}-\beta_i)+\beta_i$, we have

$$I_1=\int_{\beta_i}^{\beta_{\max}}\int_{\alpha_i}^{\alpha_{\max}} f(\alpha,\beta)d\alpha d\beta=\int_0^1\int_0^1 \bar{f}_1(\bar{\alpha},\bar{\beta})d\bar{\alpha}d\bar{\beta}, \tag{2.31}$$

inn which

$$\bar{f}_1(\bar{\alpha},\bar{\beta})=f(\bar{\alpha}(\alpha_{\max}-\alpha_i)+\alpha_i,\bar{\beta}(\beta_{\max}-\beta_i)+\beta_i)\left|J_\alpha J_\beta\right|,\ J_\alpha=\alpha_{\max}-\alpha_i \quad \text{and} \quad J_\beta=\beta_{\max}-\beta_i.$$

Next, we employ further transformation $\bar{\alpha}=\rho\cos\theta$, $\bar{\beta}=\rho\sin\theta$ and get

$$\begin{aligned} I_1&=\int_0^1\int_0^{\bar{\alpha}}\bar{f}_1(\bar{\alpha},\bar{\beta})d\bar{\beta}d\bar{\alpha}+\int_0^1\int_0^{\bar{\beta}}\bar{f}_1(\bar{\alpha},\bar{\beta})d\bar{\alpha}d\bar{\beta}\\ &=\int_0^{\pi/4}\int_0^{1/\cos\theta}\bar{f}_1(\rho\cos\theta,\rho\sin\theta)\rho d\rho d\theta\\ &\quad+\int_{\pi/4}^{\pi/2}\int_0^{1/\cos(\pi/2-\theta)}\bar{f}_1(\rho\cos\theta,\rho\sin\theta)\rho d\rho d\theta. \end{aligned} \tag{2.32}$$

Note that when (α,β) approaches (α_i,β_i), the function $f(\alpha,\beta)$ satisfies the following relationship

$$\lim_{(\alpha,\beta)\to(\alpha_i,\beta_i)} f(\alpha,\beta)=\lim_{(\alpha,\beta)\to(\alpha_i,\beta_i)}\frac{h(\alpha_i,\beta_i)}{\sqrt{k_{11}(\alpha-\alpha_i)^2+k_{12}(\alpha-\alpha_i)(\beta-\beta_i)+k_{22}(\beta-\beta_i)^2}} \tag{2.33}$$

with

$$\begin{aligned} k_{11}&=[X_{,\alpha}(\alpha_i,\beta_i)]^2+[Y_{,\alpha}(\alpha_i,\beta_i)]^2+[Z_{,\alpha}(\alpha_i,\beta_i)]^2,\\ k_{12}&=2[X_{,\alpha}(\alpha_i,\beta_i)X_{,\beta}(\alpha_i,\beta_i)+Y_{,\alpha}(\alpha_i,\beta_i)Y_{,\beta}(\alpha_i,\beta_i)+Z_{,\alpha}(\alpha_i,\beta_i)Z_{,\beta}(\alpha_i,\beta_i)], \end{aligned}$$

and

$$k_{22}=\left[X_{,\beta}(\alpha_i,\beta_i)\right]^2+\left[Y_{,\beta}(\alpha_i,\beta_i)\right]^2+\left[Z_{,\beta}(\alpha_i,\beta_i)\right]^2.$$

Thus, when $(\alpha,\beta)\to(\alpha_i,\beta_i)$, that is, $\rho\to 0$, we have

$$\begin{aligned} \lim_{\rho\to 0}\bar{f}_1(\rho\cos\theta,\rho\sin\theta)\rho&=\lim_{\rho\to 0}\frac{h(\alpha_i,\beta_i)\left|J_\alpha J_\beta\right|\rho}{\sqrt{k_{11}[J_\alpha\rho\cos\theta]^2+k_{12}J_\alpha J_\beta\rho^2\cos\theta\sin\theta+k_{22}[J_\beta\rho\sin\theta]^2}}\\ &=\frac{h(\alpha_i,\beta_i)\left|J_\alpha J_\beta\right|}{\sqrt{k_{11}[J_\alpha\cos\theta]^2+k_{12}J_\alpha J_\beta\cos\theta\sin\theta+k_{22}[J_\beta\sin\theta]^2}}. \end{aligned} \tag{2.34}$$

From Eq. (2.34), we can observe that the singularity of $f(\alpha,\beta)$ is eliminated by the above transformation.

Then the integration I_1 is calculated by using Gauss quadrature as

$$I_1=\sum_{n=1}^{N_G} w_n\frac{\pi}{8}\Big(\sum_{m=1}^{N_G} w_m g_1(\hat{\rho}_m,\hat{\theta}_n)\frac{1}{2\cos\hat{\theta}_n}\Big) + \sum_{n=1}^{N_G} w_n\frac{\pi}{8}\Big(\sum_{m=1}^{N_G} w_m g_1(\bar{\rho}_m,\bar{\theta}_n)\frac{1}{2\cos(\pi/2-\bar{\theta}_n)}\Big), \tag{2.35}$$

where

$$g_1(\rho,\theta)=f(\rho\cos(\theta)J_\alpha+\alpha_i,\rho\sin(\theta)J_\beta+\beta_i)\big|J_\alpha J_\beta\big|\rho,\quad \hat{\theta}_n=\frac{\pi}{8}+\kappa_n\frac{\pi}{8},$$
$$\bar{\theta}_n=\frac{3\pi}{8}+\kappa_n\frac{\pi}{8},\quad \hat{\rho}_m=\frac{1}{2}\left(\frac{1}{\cos\hat{\theta}_n}+\frac{1}{\cos\hat{\theta}_n}\kappa_m\right),$$
$$\bar{\rho}_m=\frac{1}{2}\left[\frac{1}{\cos(\pi/2-\bar{\theta}_n)}+\frac{1}{\cos(\pi/2-\bar{\theta}_n)}\kappa_m\right],$$

with κ_m the mth the Gauss point, w_m the weighted function, and N_G the number of Gauss points.

Similarly, the remaining integration can be calculated by using the following transform

$$\begin{aligned}
&\alpha=\rho\cos(\theta)(\alpha_{\min}-\alpha_i)+\alpha_i, && \beta=\rho\sin(\theta)(\beta_{\max}-\beta_i)+\beta_i \quad \text{for } I_2,\\
&\alpha=\rho\cos(\theta)(\alpha_{\min}-\alpha_i)+\alpha_i, && \beta=\rho\sin(\theta)(\beta_{\min}-\beta_i)+\beta_i \quad \text{for } I_3,\\
&\alpha=\rho\cos(\theta)(\alpha_{\max}-\alpha_i)+\alpha_i, && \beta=\rho\sin(\theta)(\beta_{\min}-\beta_i)+\beta_i \quad \text{for } I_4,
\end{aligned}$$

which leads to a unified form

$$I_i=\int_0^{\pi/4}\int_0^{1/\cos\theta} f(\rho\cos(\theta)J_\alpha+\alpha_i,\rho\sin(\theta)J_\beta+\beta_i)\big|J_\alpha J_\beta\big|\rho d\rho d\theta + \int_{\pi/4}^{\pi/2}\int_0^{1/\cos(\pi/2-\theta)} f(\rho\cos(\theta)J_\alpha+\alpha_i,\rho\sin(\theta)J_\beta+\beta_i)\big|J_\alpha J_\beta\big|\rho d\rho d\theta,\quad (i=2,3,4),$$

with $J_\alpha=(\alpha_{\min}-\alpha_i)$, $J_\beta=(\beta_{\max}-\beta_i)$ for I_2, $J_\alpha=(\alpha_{\min}-\alpha_i)$, $J_\beta=(\beta_{\min}-\beta_i)$ for I_3, and $J_\alpha=(\alpha_{\max}-\alpha_i)$, $J_\beta=(\beta_{\min}-\beta_i)$ for I_4. Then I_2, I_3 and I_4 can be calculated via the Gauss quadrature like Eq. (2.35).

Particularly, if $f(\alpha,\beta)$ is a periodic function in term of α, i.e., $f(\alpha_{\min},\beta)=f(\alpha_{\max},\beta)$, the integration interval $[\alpha_{\min},\alpha_{\max}]$ of Eq. (2.29) should be transformed into $\left[\alpha_i-\frac{\alpha_{\max}-\alpha_{\min}}{2},\alpha_i+\frac{\alpha_{\max}-\alpha_{\min}}{2}\right]$ to avoid nearly-singular integration. Similarly, the similar transformation need to be applied for the variable β, if $f(\alpha,\beta)$ is a periodic function in term of β.

3 Numerical results

In this section, four 3D examples are presented to illustrate the convergence, accuracy and flexibility of the proposed techniques to evaluate the OIFs in the SBM. The first two examples are concerned with spherical and cubic domains subject to discontinuous Dirichlet and mixed-type boundary conditions, respectively. The remaining two examples are involved with complicated-shaped domains subject to continuous boundary conditions. A comparison is made with the MFS, the SBM based on inverse interpolation technique (IIT SBM) [12], and the BEM to assess the validity of the present SBM. In the MFS, we use the following formula to obtain the source points:

$$\mathbf{s}_i = \mathbf{x}_i^b + d\mathbf{n}_x^b,$$

where $\mathbf{x}_i^b$ is the point chosen from the boundary, $\mathbf{n}_x^b$ represents the unit outward normal at $\mathbf{x}_i^b$ and $d>0$ denotes the distance between the source points and the physical boundary. It is worth noting that the location of the source points usually affects the accuracy of the MFS. Recently, some new studies suggest how to place the source points, and the interested readers are referred to [24–27]. In the BEM, the direct formulation introduced in [28] is adopted and the integrations of the fundamental solution and its normal gradient over each element are calculated through 9-point Gauss quadrature. To assess the accuracy of the present method, the following average relative error is defined by

$$Rerr = \sqrt{\frac{\sum_{k=1}^{nt}\left[\xi(\mathbf{x}_k)-\bar{\xi}(\mathbf{x}_k)\right]^2}{\sum_{k=1}^{nt}\xi^2(\mathbf{x}_k)}}, \quad \xi = \left\{u, \frac{\partial u}{\partial x_i}\right\}, \tag{3.1}$$

where $\xi(\mathbf{x}_k)$ and $\bar{\xi}(\mathbf{x}_k)$ are exact and numerical results at the test point $\mathbf{x}_k$, respectively, and nt denotes the number of test points. The implementation uses Matlab R2007a on a single Intel Core(TM) processor running at 2.1GHz with 2MB L2 cache of a dual CPU workstation having a total of 2GB DDR2 memory.

3.1 Spherical domain case

The first example considers a spherical domain of radius 1 centered at the origin. The discontinuous Dirichlet boundary conditions

$$\bar{u} = \begin{cases} 0, & x_3 > 0, \\ 1, & x_3 \le 0, \end{cases} \qquad \mathbf{x} \in \Gamma,$$

is imposed on the whole boundary. The corresponding analytical solution in spherical coordinates with $(x_1,x_2,x_3) = (r\sin(\theta)\cos(\phi), r\sin(\theta)\sin(\phi), r\cos(\theta))$, $0 \le \theta \le \pi$, $0 \le \phi \le 2\pi$ is given by

$$u(r,\theta) = \sum_{n=0}^{\infty} A_n r^n P_n(\cos(\theta)),$$

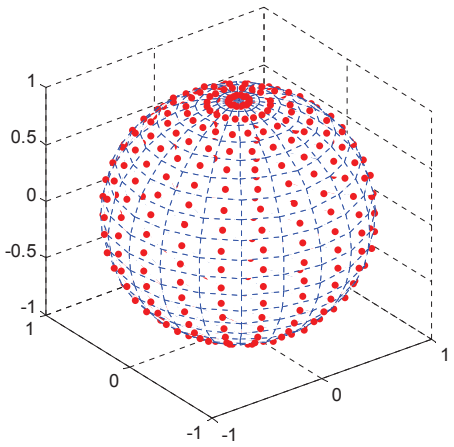

Figure 2: The sketch of the source point distribution ($N=400$).

where P_n is the nth Legendre polynomial, $A_0=0.5$, $A_1=-0.75$ and

$$A_n=\frac{a_{n+1}-b_{n+1}-a_{n-1}+b_{n-1}}{2},\quad (n=2,3,\cdots),$$

with

$$b_n=(-1)^n,\quad a_n=\begin{cases}0, & n=1,3,5,7,\cdots,\\ \dfrac{(-1)^{n/2}n!}{2^n[(n/2)!]^2}, & n=0,2,4,6,\cdots.\end{cases}$$

The sketch distribution of 400 source points on the boundary surface is shown in Fig. 2. To show the numerical solution accuracy, 100 test points are chosen from the surface of a sphere of radius 0.7 with center at origin.

Fig. 3 shows the average relative errors by the BEM, MFS and SBM. It can be seen that the MFS with $d=0.5$ performs better than the other methods. But the MFS results in undesirable or unstable numerical solutions when the source points are distributed near, i.e., $d=0.05$, or far, i.e., $d=1$, from the physical boundary. Thus the accuracy and stability of the MFS are strongly influenced by the location of the auxiliary boundary. It is noted that the MFS even with the appropriate auxiliary boundary has no obvious advantages over the present SBM. This indicates that the present method is more suitable than the MFS for this discontinuous boundary condition problem.

Furthermore, we can observe that the SBM using the IIT and the proposed technique for OIFs results in the similar accuracy of solutions. The condition numbers of the linear systems generated by the BEM, MFS and SBM are plotted in Fig. 4. It is noted that the condition numbers of the BEM and the SBMs are in the same order of magnitude and are clearly smaller than that of the MFS with the same number of the source points. This

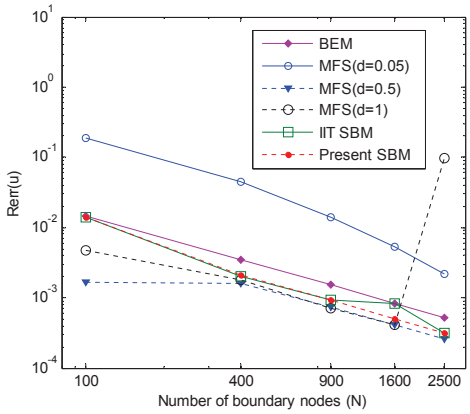

Figure 3: Average relative errors by the BEM, MFS and SBM for a spherical domain problem.

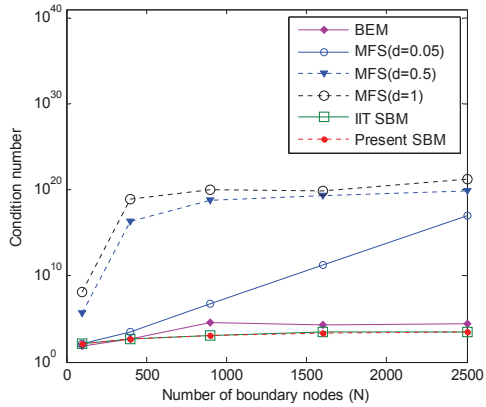

Figure 4: Condition numbers of the linear equations generated by the BEM, MFS and SBM for a spherical domain problem.

shows good stability of the present SBM scheme. Particularly, the largest condition number of the MFS with $d=1$ illustrates that its influence matrix is ill-conditioned and gives rise to the instable solution. The CPU time by the BEM, MFS and SBM is listed in Table 1. It can be found that the present SBM for this problem uses less time than the other methods with the same number of source points.

3.2 Cubic domain case

This section investigates on a problem in a cubic domain covering $0\leq x_1,x_2,x_3\leq 1$. The following mixed boundary conditions are prescribed on the boundary

$$u(1,x_2,x_3)=1.5+x_2x_3,\quad u(x_1,1,x_3)=3+x_1x_3,\quad u(x_1,x_2,1)=2+x_1x_2,$$
$$q(0,x_2,x_3)=q(x_1,0,x_3)=q(x_1,x_2,0)=0.$$

Table 1: CPU time used by the BEM, MFS and SBM for spherical domain problem (in seconds).

N	BEM	MFS ($d=0.5$)	IIT SBM	Present SBM
100	0.25	0.046	0.061	0.046
400	1.50	0.128	0.243	0.131
900	6.32	0.488	1.168	0.447
1600	18.81	1.654	3.717	1.400
2500	44.78	4.717	10.27	3.726

An analytical solution is available as follows

$$u(\mathbf{x})=u_1+u_2+u_3,$$

where

$$u_1=\sum_{i=0}^{\infty}\sum_{j=0}^{\infty}a_{ij}\cosh\left(\sqrt{k_i^2+k_j^2}x_1\right)\cos(k_ix_2)\cos\left(k_jx_3\right),$$
$$u_2=\sum_{m=0}^{\infty}\sum_{l=0}^{\infty}b_{ml}\cosh\left(\sqrt{g_m^2+g_l^2}x_2\right)\cos(g_mx_1)\cos(g_lx_3),$$
$$u_3=\sum_{t=0}^{\infty}\sum_{p=0}^{\infty}c_{tp}\cosh\left(\sqrt{h_t^2+h_p^2}x_3\right)\cos(h_tx_1)\cos\left(h_px_2\right),$$

with

$$k_i=(i+0.5)\pi,\qquad a_{ij}=4\left[1.5\frac{(-1)^{i+j}}{k_ik_j}+\left(\frac{(-1)^i}{k_i}-\frac{1}{k_i^2}\right)\left(\frac{(-1)^j}{k_j}-\frac{1}{k_j^2}\right)\right]\Big/\cosh\left(\sqrt{k_i^2+k_j^2}\right),$$
$$g_m=(m+0.5)\pi,\quad b_{ml}=4\left[3\frac{(-1)^{m+l}}{g_mg_l}+\left(\frac{(-1)^m}{g_m}-\frac{1}{g_m^2}\right)\left(\frac{(-1)^l}{g_l}-\frac{1}{g_l^2}\right)\right]\Big/\cosh\left(\sqrt{g_m^2+g_l^2}\right),$$
$$h_t=(t+0.5)\pi,\qquad c_{tp}=4\left[2\frac{(-1)^{t+p}}{h_mh_p}+\left(\frac{(-1)^t}{h_t}-\frac{1}{h_t^2}\right)\left(\frac{(-1)^p}{h_p}-\frac{1}{h_p^2}\right)\right]\Big/\cosh\left(\sqrt{h_t^2+h_p^2}\right).$$

The source points are uniformly distributed on the boundary surface. 100 test points are chosen from the surface of a sphere with radius 0.475 centered at $(0.5,0.5,0.5)$.

Fig. 5 illustrates the average relative errors versus number of boundary nodes. It can be seen that the MFS with $d=0.05$ has larger error than the one with $d=0.5$. Moreover, the MFS results with $d=1$ appears not stable. Once again, we see that the location of the auxiliary boundary is vital to accuracy and stability of the MFS solutions. From Fig. 5 we also notice that the SBM with the IIT has a little better accuracy than the SBM with the proposed technique for OIFs when the number of boundary source nodes N is less than 2400, but it becomes a little worse when N reaches 2400. This indicates that the proposed technique performs more stable and accurate than the IIT for large scale problems.

The CPU time by the BEM, the MFS and the SBM is provided in Table 2. It can be seen that the present SBM scheme consumes more time than the MFS but appears more

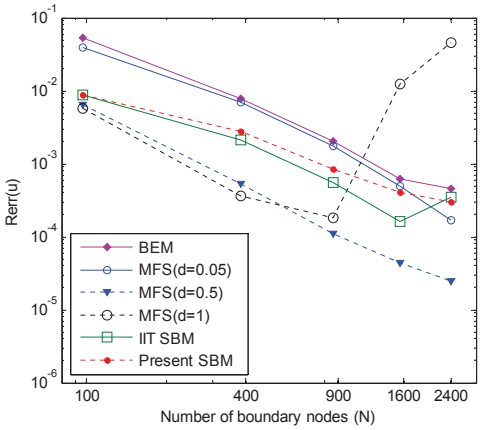

Figure 5: Average relative errors by BEM, MFS, SBM for a cubic domain problem.

efficient than the SBM with the IIT and the BEM using the same number of the boundary nodes.

3.3 Bean-shaped domain case

This case is concerned with a bean-shaped domain [14] having the surface as shown in Fig. 6

$$\frac{x_1^2}{0.64\left(1-0.1\cos\left(\frac{\pi x_3}{R}\right)\right)}+\frac{\left(x_2+0.3\cos\left(\frac{\pi x_3}{R}\right)\right)^2}{0.64\left(1-0.4\cos\left(\frac{\pi x_3}{R}\right)\right)}+x_3^2=R^2,$$

where $R=1$. The analytical solution is

$$u(\mathbf{x})=\exp\left(\sqrt{2}x_3\right)\cos(x_1)\sin(x_2)+2x_1+2x_2+2x_3+1. \tag{3.2}$$

Unlike the previous two examples, the integration of fundamental solution over the whole boundary cannot be analytically computed in this case. Therefore, the method presented in case 4 of Section 2.3 is employed. The number of the Gauss points in Eq. (2.35) is

Table 2: CPU time used by the BEM, MFS and SBM for cubic domain problem (in seconds).

N	BEM	MFS ($d=0.5$)	IIT SBM	Present SBM
96	2.674	2.445	2.429	2.411
384	4.458	2.677	2.782	2.763
864	10.012	3.195	3.757	3.533
1536	23.452	4.628	6.734	5.768
2400	50.390	8.132	13.893	10.697

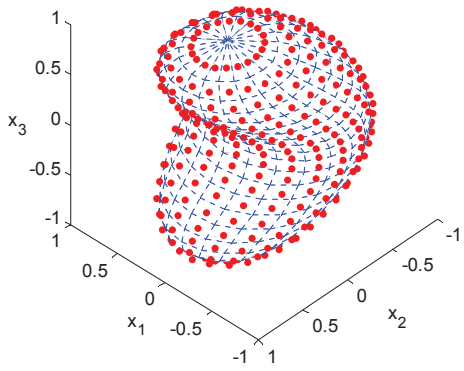

Figure 6: The sketch of the source point distribution.

set to be $N_G = 10$. The sketch distribution of 400 source points on the boundary is shown in Fig. 6. 100 evenly distributed test points are chosen on the circle ($x_3 = 0$) with radius of 0.4 centered at $(0, -0.3)$.

Figs. 7(a)-(d) display the curves of relative average errors of u and $\partial u/\partial x_i$ $(i = 1,2,3)$ by the MFS, the SBM and the BEM. It can be seen that the MFS with $d = 0.5$ which is valid in the previous two examples converges quickly when the number of boundary nodes N is small but becomes unstable when N is over 1600. Thus, the location of the appropriate auxiliary boundaries depends on the practical problems of interest, which limits its applicability for the practical engineering problems. It can be observed from Figs. 7 that the SBM with the proposed technique and the IIT obtains similarly accurate results. Table 3 provides the CPU time. It is noted that the present SBM formulation needs more time than the MFS but obviously use less time than the BEM. Furthermore, the proposed technique for OIFs uses less time than the IIT in the SBM when the number of the boundary nodes is over 900. This indicates the validity of the present method.

3.4 Complicated domain cases

To further verify the capability of the present SBM formulation in solving the complicated domain problems, *L*-shaped, toroidal and hollow circular cylindrical [12] domains are considered.

Table 3: CPU time in the BEM, MFS and SBM for bean-shaped domain (in seconds).

N	BEM	MFS ($d = 0.5$)	IIT SBM	Present SBM
100	0.439	0.0623	0.0730	0.174
400	2.406	0.271	0.386	0.627
900	8.672	0.833	1.446	1.571
1600	23.449	2.254	4.331	3.438
2500	54.005	5.663	11.261	7.031

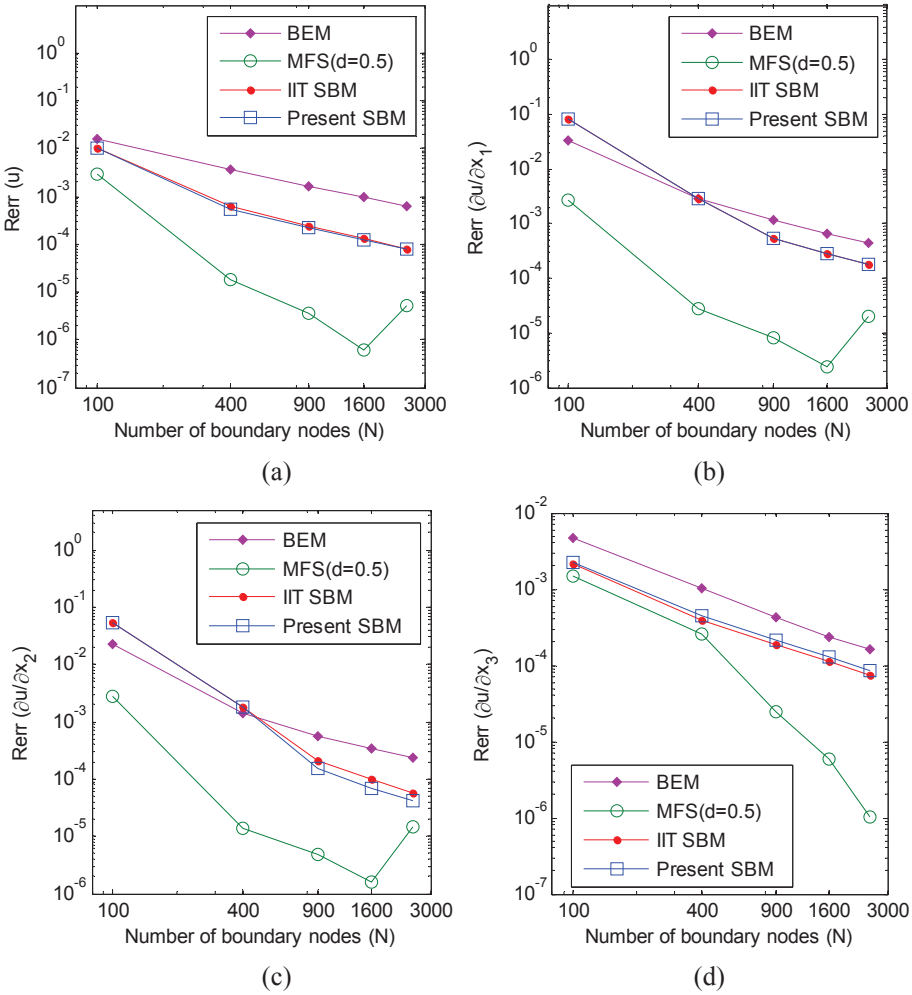

Figure 7: Average relative errors of (a) u, (b) $\partial u/\partial x_1$, (c) $\partial u/\partial x_2$ and (d) $\partial u/\partial x_3$ for a bean-shaped domain problem.

The L-shaped domain is given by $\Omega^{(1)}=\Omega_1\cup\Omega_2$, where $\Omega_1=[0,1]\times[0,0.5]\times[0,0.5]$ and $\Omega_2=[0,0.5]\times[0.5,1]\times[0,0.5]$. The toroidal and hollow circular cylindrical domains are respectively represented by

$$\Omega^{(2)}=\{\mathbf{x}=(f(\phi)\cos\theta,f(\phi)\sin\theta,\rho\sin\phi)\,|\,f(\phi)=4+\rho\cos\phi,\ 0\le\theta,\phi<2\pi,\ 0\le\rho\le1\},$$

and

$$\Omega^{(3)}=\{\mathbf{x}=(\rho\cos\theta,\rho\sin\theta,x_3)\,|\,1\le\rho\le2,\ 0\le\theta<2\pi,\ -2\le x_3\le2\}.$$

The analytical solutions of the three cases are function (3.2). The Dirichlet boundary conditions are prescribed on the whole boundaries of the L-shaped and toroidal domains,

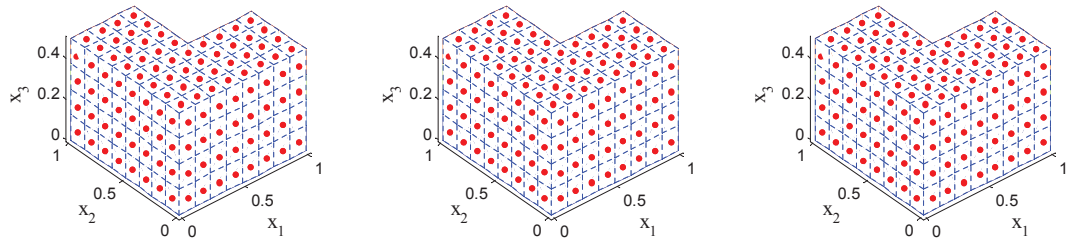

Figure 8: The distribution of source points on (a) the L-shaped domain ($N=224$), (b) the torus ($N=432$) and (c) the hollow circular cylinder ($N=648$).

and the mix-type boundary conditions are imposed on the boundary of hollow circular cylindrical domain with the Neumann boundary conditions prescribed on the upper and lower surfaces and the Dirichlet boundary conditions specified on the rest of the boundary. The methods presented in cases 2, 3 and 4 of Section 2.3 are used to calculate the integration of the fundamental solution over the boundaries of L-shaped, hollow circular cylindrical and toroidal domains, respectively. The numbers of the Gauss points are set to be $N_G=18$ for case 3 and $N_G=10$ for case 4. To assess the convergence rate of the present method, the following formulations [14] are considered

$$C=-2\frac{\ln(Error(N_1))-\ln(Error(N_2))}{\ln(N_1)-\ln(N_2)},$$

where $Error(N_1)$ and $Error(N_2)$ represent the errors ($Rerr(\xi)$) of the present SBM with N_1 and N_2 boundary nodes.

Figs. 8(a)-(c) display the distribution of the source points on the surface of the three different geometries of interest. 100 test points are chosen from the surface of a sphere of radius 0.2 centered at $(0.25,0.25,0.25)$ for the L-shaped domain, and 100 points from two different circles on the plane $x_3=0$ with the same centers at origin having radius 4 and 1.6 for the toroidal and hollow circular cylindrical domains, respectively. Figs. 9(a)-(c) plot the convergence curve of u and $\partial u/\partial x_i$ of the present SBM for the three different problems. It can be observed that the convergence rates of the present SBM for the three problems are around 2 which implies that the present method is robust for the complex-shaped problems.

4 Conclusions

The SBM is a recently developed boundary-type strong-form meshless method which approximates the solution of the problem by the combination of the fundamental solutions and introduces the concept of OIFs to avoid the singularities at origins. In the standard SBM formulation, the OIFs on Neumann boundary can be efficiently derived

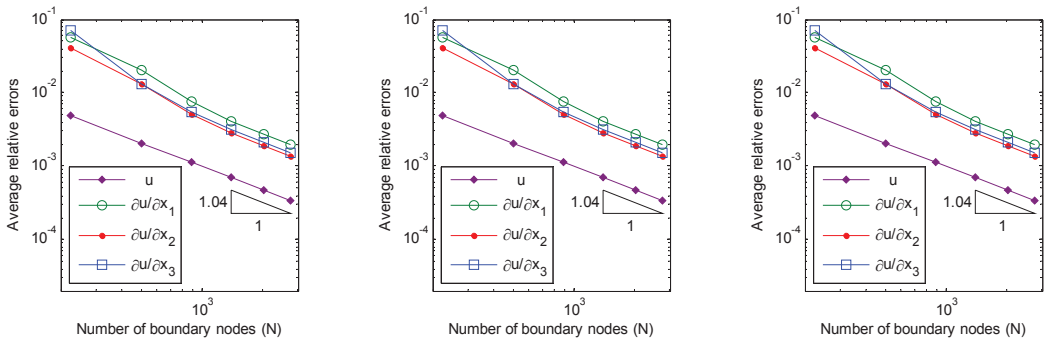

Figure 9: Average relative errors by the present SBM for the problems under (a) L-shaped, (b) toroidal, and (c) hollow circular cylinder domains, respectively.

by a subtracting and adding-back technique, but the calculation of the OIFs on Dirichlet boundary is more complicated and time-consuming.

This study presents a new formula for the OIFs on three-dimensional Dirichlet boundary. The technique adopts the subtracting and adding-back technique based on the integration of the fundamental solution over the whole boundary. The proposed formulation remedies the major drawbacks in the standard inverse interpolation technique. The numerical experiments demonstrate that the present SBM formulation has quadratic convergence rate. In addition, the comparison with the MFS, BEM and the standard SBM based on IIT shows that the present method is accurate, stable and efficient.

Appendix

A Detailed derivation of Eq. (2.7)

The null-field of the boundary integral equation (BIE) based on the direct method is given by

$$\int_\Gamma \frac{\partial G^{(e)}(\mathbf{x}_m,\mathbf{s})}{\partial \mathbf{n}_s} u^L - \frac{\partial u^L}{\partial \mathbf{n}_s} G^{(e)}(\mathbf{x}_m,\mathbf{s}) d\Gamma(\mathbf{s}) = 0, \quad \mathbf{x}_m \in \Omega^{(e)}, \tag{A.1}$$

where the superscript (e) denotes the exterior domain, $G^{(e)}(\mathbf{x}_m,\mathbf{s})$ is the fundamental solution for the potential problem in exterior domain, $\mathbf{s}$ represents the source point on the boundary, and $\mathbf{x}_m$ denotes the field point in the exterior domain. Let $u^L = 1$, we can rewrite Eq. (A.1) as follows

$$\int_\Gamma \frac{\partial G^{(e)}(\mathbf{x}_m,\mathbf{s})}{\partial \mathbf{n}_s} d\Gamma(\mathbf{s}) = 0. \tag{A.2}$$

When $\mathbf{x}_m$ approaches the boundary, we discretize the Eq. (A.2) by

$$\int_\Gamma \frac{\partial G^{(e)}(\mathbf{x}_m,\mathbf{s})}{\partial \mathbf{n}_s} d\Gamma(\mathbf{s}) = \sum_{j=1}^{N} \int_{\Gamma_j} \frac{\partial G^{(e)}(\mathbf{x}_m,\mathbf{s})}{\partial \mathbf{n}_s} d\Gamma_j(\mathbf{s}) \approx \sum_{j=1}^{N} L_j \frac{\partial G^{(e)}(\mathbf{x}_m,\mathbf{s}_j)}{\partial \mathbf{n}_s} = 0, \tag{A.3}$$

where L_j denotes the area of the curved surface containing $\mathbf{s}_j$, as shown in Fig. 1. Then, we have

$$\sum_{j=1}^{N} \frac{L_j}{L_m} \frac{\partial G^{(e)}(\mathbf{x}_m,\mathbf{s}_j)}{\partial \mathbf{n}_s} = 0.$$

Acknowledgments

The work described in this paper was supported by the National Science Funds for Distinguished Young Scholars of China (No. 11125208), NSFC Funds (Nos. 11302069, 11372097, 11602114 and 11662003), the 111 project under Grant No. B12032.

References

[1] W. CHEN AND F. Z. WANG, *A method of fundamental solutions without fictitious boundary,* Eng. Anal. Bound. Elem., 34 (2010), pp. 530–532.

[2] W. CHEN, *Singular boundary method: a novel, simple, meshfree, boundary collocation numerical method,* Chinese J. Solid Mech., 30(6) (2009), pp. 592–599 (in Chinese).

[3] S. NINTCHEU FATA, *Explicit expressions for 3D boundary integrals in potential theory,* Int. J. Numer. Methods Eng., 78(1) (2009), pp. 32–47.

[4] C. A. BREBBIA, J. C. F. TELLES AND L. C. L. WROBEL, Boundary Element Techniques: Theory and Applications in Engineering, Springer, New York, 1984.

[5] A. H. D. CHENG AND D. T. CHENG, *Heritage and early history of the boundary element method,* Eng. Anal. Bound. Elem., 29 (2005), pp. 268–302.

[6] G. FAIRWEATHER AND A. KARAGEORGHIS, *The method of fundamental solutions for elliptic boundary value problems,* Adv. Comput. Math., 9 (1998), pp. 69–95.

[7] M. A. GOLBERG AND C. S. CHEN, *The method of fundamental solutions for potential, helmholtz and diffusion problems,* In M.A. Golberg, editor, Boundary Integral Methods–Numerical and Mathematical Aspects, pages 103176, Computational Mechanics Publications, Southhampton, 1998.

[8] A. KARAGEORGHIS, D. LESNIC AND L. MARIN, *A survey of applications of the MFS to inverse problems,* Inverse Probl. Sci. Eng., 19(3) (2011), pp. 309–336.

[9] W. CHEN AND Y. GU, *An improved formulation of singular boundary method,* Adv. Appl. Math. Mech., 4(5) (2012), pp. 543–558.

[10] Y. LIU AND F. J. RIZZO, *A weakly singular form of the hypersingular boundary integral equation applied to 3-D acoustic wave problems*, Comput. Methods Appl. Mech. Eng., 96(2) (1992), pp. 271–287.

[11] V. SLADEK, J. SLADEK AND M. TANAKA, *Regularization of hypersingular and nearly singular integrals in the potential theory and elasticity,* Int. J. Numer. Methods Eng., 36 (1993), pp. 1609–1628.

[12] Y. GU, W. CHEN AND X. Q. HE, *Singular boundary method for steady-state heat conduction in three dimensional general anisotropic media,* Int. J. Heat Mass Transfer, 55 (2012), pp. 4837–4848.
[13] Y. GU AND W. CHEN, *Infinite domain potential problems by a new formulation of singular boundary method,* Appl. Math. Model., 37 (2013), pp. 1638–1651.
[14] Z. J. FU, W. CHEN AND Y. GU, *Burton-Miller type singular boundary method for acoustic radiation and scattering,* J. Sound Vib., 333(16) (2014), pp. 3776–3793.
[15] J. LIN, W. CHEN AND C. S. CHEN, *Numerical treatment of acoustic problems with boundary singularities by the singular boundary method,* J. Sound Vib., 333(14) (2014), pp. 3177–3188.
[16] W. CHEN, J. Y. ZHANG AND Z. J. FU, *Singular boundary method for modified Helmholtz equations,* Eng. Anal. Bound. Elem., 44 (2014), pp. 112–119.
[17] W. Z. QU AND W. CHEN, *Solution of two-dimensional Stokes flow problems using singular boundary method,* Adv. Appl. Math. Mech., 7(1) (2015), pp. 13–30.
[18] C. YANG AND X. L. LI, *Meshless singular boundary methods for biharmonic problems,* Eng. Anal. Bound. Elem., 56 (2015), pp. 39–48.
[19] X. WEI, W. CHEN, B. CHEN AND L. L. SUN, *Singular boundary method for heat conduction problems with certain spatially varying conductivity,* Comput. Math. Appl., 69 (2015), pp. 206–222.
[20] X. WEI, W. CHEN, L. SUN AND B. CHEN, *A simple accurate formula evaluating origin intensity factor in singular boundary method for two-dimensional potential problems with Dirichlet boundary,* Eng. Anal. Bound. Elem., 58(0) (2015), pp. 151–165.
[21] W. CHEN, Z. J. FU AND X. WEI, *Potential problems by singular boundary method satisfying moment condition,* Comput. Model. Eng. Sci., 54 (2009), pp. 65–86.
[22] D. L. YOUNG, K. H. CHEN AND C. W. LEE, *Novel meshless method for solving the potential problems with arbitrary domain,* J. Comput. Phys., 209 (2005), pp. 290–321.
[23] L. L. SUN, W. CHEN AND C. Z. ZHANG, *A new formulation of regularized meshless method applied to interior and exterior anisotropic potential problems,* Appl. Math. Model., 37(12) (2013), pp. 7452–7464.
[24] R. SCHABACK, *Adaptive numerical solution of MFS systems*, In C.S. Chen, A. Karageorghis, Y. S. Smyrlis, eds., The Method of Fundamental Solutions–A Meshless Method, pages 1–27, Dynamic Publishers, Inc., Atlanta, 2008.
[25] T. SHIGETA, D. L. YOUNG AND C. S. LIU, *Adaptive multilayer method of fundamental solutions using a weighted greedy QR decomposition for the Laplace equation,* J. Comput. Phys., 231 (2012), pp. 7118–7132.
[26] M. LI, C. S. CHEN AND A. KARAGEORGHIS, *The MFS for the solution of harmonic boundary value problems with non-harmonic boundary conditions,* Comput. Math. Appl., 66 (2013), pp. 2400–2424.
[27] C. S. CHEN, A. KARAGEORGHIS AND YAN LI, *On choosing the location of the sources in the MFS,* Numer. Algorithms, 72 (2016), pp. 107–130.
[28] P. K. BANERJEE, The Boundary Element Methods in Engineering, McGRAW-HILL Book Company, Europe, 1994.